1. Large Helical Device (LHD) Project

The Large Helical Device (LHD) project conducts fusion-grade confinement research in a steady-state machine to elucidate important research issues in physics and engineering for the helical-type fusion reactor.

The LHD is one of the largest helical devices, with major and averaged minor radii of 3.6 – 4.0 m and 0.6 m, respectively. A double helical coil and three pairs of poloidal coils are all superconducting, by which maximum magnetic field strength at the plasma center is 3 T. For plasma heating, three negative-ion-based 180 – 190 keV neutral beams with total heating power of 8 – 16 MW are injected tangentially to the plasma.

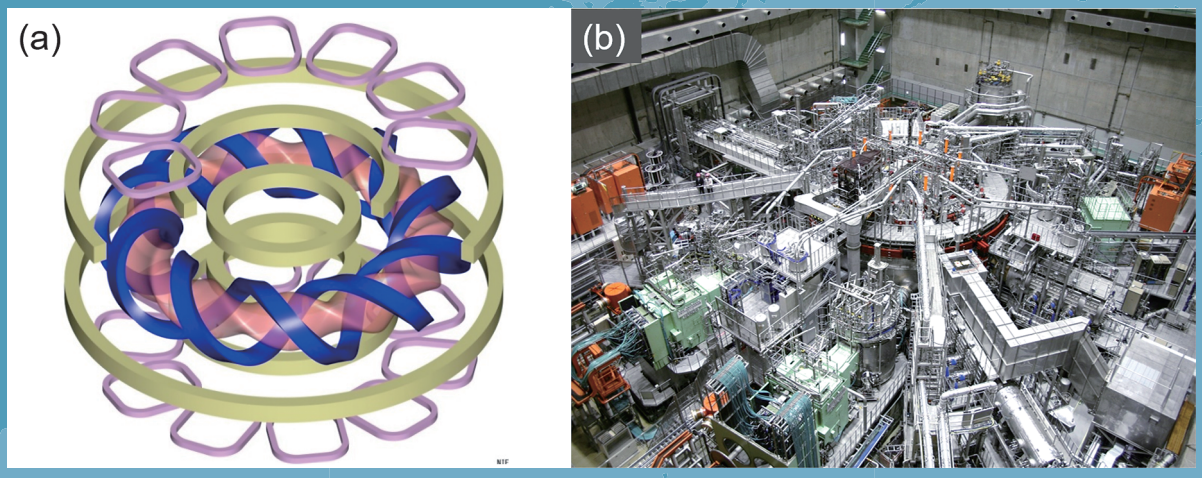

Fig. 1 (a) Coil configuration of LHD. Superconducting helical coils (blue), poloidal coils (yellow) and normal conducting RMP coils, together with plasma. (b) LHD torus hall.

Two positive-ion-based 40 – 80 keV neutral beams with total heating power of 6 – 18 MW are also injected perpendicular to the plasma. In addition, electron cyclotron resonance heating with total heating power of ~ 5.5 MW is also available. For fuelling, LHD is equipped with four gas puff valves and two pellet injectors.

Since 2017, LHD has performed the deuterium experiment in which plasma is expected to improve its performance, thanks to the "isotope effect". Achieved plasma parameters to date are summarized in Table 1.

Table 1 Achieved plasma parameters (1998 – 2017).

Parameters	Achieved	Key physics	Target
T_i	10 keV ($n_e = 1.3\times10^{19}$ m^{-3})	Ion ITB Impurity hole	10 keV ($n_e = 2\times10^{19}$m^{-3})
T_e	20 keV (2×10^{18} m^{-3}) 10 keV (1.6×10^{19} m^{-3})	Electron ITB	10 keV (2×10^{19}m^{-3})
Density	1.2×10^{21}m^{-3} ($T_e = 0.25$ keV)	Super dense core	4×10^{20} m^{-3} ($T_e = 1.3$ keV)
β	5.1 % ($B_T = 0.425$ T) 4.1 % (1 T)	MHD in current-free plasmas	5 % ($B_T = 1$ - 2 T)
Steady-state operation	54min. 28sec (0.5MW, 1keV, 4×10^{18}m^{-3}) 47min. 39sec. (1.2MW, 2keV, 1×10^{19}m^{-3})	Dynamic wall retention	1 hour (3 MW)

(T. Morisaki)

High Performance Plasma

Highlight

The isotope effect of ion thermal confinement of high ion temperature plasmas with ion internal transport barrier was investigated, and the study on energetic particles progressed.

A remarkable extension of high-ion-temperature regime was obtained in deuterium (D) plasma experiments in the LHD [1]. The dependence of the ion heat diffusivity on temperature ratio T_e/T_i and the inverse of the normalized scale length of the ion temperature gradient R/L_{Ti} was investigated in the core region [2], where the gyrokinetic simulations using GKV code predict the destabilization of ion temperature gradient (ITG) modes [3]. The T_e/T_i dependence shows ITG-like property, while a significant deviation from the ITG-like property is found in the R/L_{Ti} dependence as shown in Fig. 1. The ion heat diffusivity normalized by gyroBohm factor tended to decrease with increasing R/L_{Ti}. This indicates the suppression of ITG mode in large R/L_{Ti} regime and results in the formation of the ion internal transport barrier (ITB). In the comparison between D and hydrogen (H) plasmas, the lower transport in D plasmas were observed in both ion and electron heat diffusivities, indicating significant isotope effect. It was found with the nonlinear turbulent transport simulation with GKV that the zonal flow enhancement contributes to the ITG suppression in the D plasmas.

Research on energetic particle (EP) confinement has advanced using comprehensive neutron diagnostics prepared for D operation of the LHD plasma [4]. The fusion gain Q_{DD} is evaluated to be 4.0×10^{-4} in the N-NB-heated D plasma, which is comparable with Q_{DD} obtained in large tokamaks with similar heating power. The ratio of Q_{DT}/Q_{DD} is evaluated by means of the FBURN code [5] using the experimental data. We achieved the equivalent Q_{DT} of 0.11.

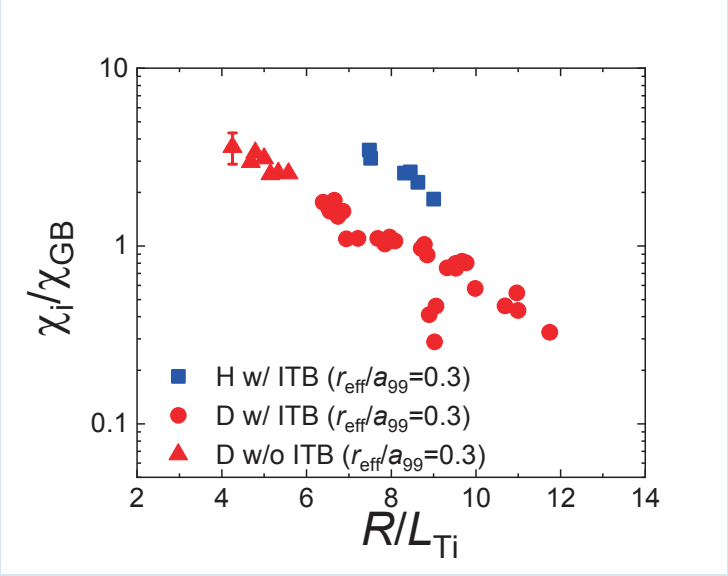

Fig. 1 The ion heat diffusivity normalized by gyroBohm factor as a function of temperature normalized ion temperature gradient at $r_{eff}/a_{99} = 0.3$ [2].

Transport characteristics of D and H plasmas with ion internal transport barrier in the LHD

The D plasma experiments were started in the 19th experimental campaign in 2017. The isotope effects in the core of high-ion-temperature plasma have been investigated in this study. In order to minimize the multi-ion-species effects on ion heat transport, the H and the D plasmas with high-ion-purity were produced and analyzed in this study. The purity of the ion species is over 80% for both plasmas: $n_D/n_e > 0.8$ or $n_H/n_e > 0.8$. The effective charge Z_{eff} was less than 2 in the core region due to the formation of impurity hole. The plasmas were heated with NBIs. The D beams were injected to the D plasmas and the H beams were injected to the H plasmas. The dominant instability in the core region of the high-T_i plasmas is ITG mode [6]. The ITG mode is mainly characterized with R/L_{Ti} and T_e/T_i. The ion heat diffusivity normalized by gyroBohm factor χ_i/χ_{GB} was found to be increased with the temperature ratio. The dependence is consistent with the ITG nature. On the other hand, the χ_i/χ_{GB} decreases with R/L_{Ti} as shown in Fig. 1. This is the opposite tendency to the ITG nature and the transport improves with increase of R/L_{Ti}. The ion ITB formation is attributable to the transport improvement with the breaking of R/L_{Ti} dependence of ITG mode. The difference of transport levels between H and D plasmas can also be seen, although the dependence on R/L_{Ti} was similar between them. This observation suggests that the mechanism of transport improvement is related to some parameters depending on ion mass. The difference in the Larmor radius between H and D might provide an explanation of the experimental observation.

The nonlinear turbulent transport simulations using the GKV code [7] were conducted in order to discuss physical mechanisms of the isotope effect observed in the experiment. The calculation showed the destabilization of the ITG mode in the plasma core both in the H and D plasmas. Figure 2 shows the time evolution of the normalized heat diffusivity at the half minor radius. The turbulent transport was saturated after growth of zonal flow. The saturation level of the turbulent transport in the H plasma is higher than that of the experimental value ($\chi_i/\chi_{GB,H}$ ~10). When the temperature gradient was artificially reduced by 20% in the simulation, the turbulent transport level became almost the experimental value as the dashed line showed in Fig. 2 (a), indicating that the turbulent transport simulation reproduced the ion heat diffusivity within 20% variations from the nominal value of experimentally observed ion temperature gradient. In the estimation of experimental heat diffusivities, the uncertainty is 25% at maximum, which is mainly due to an evaluation of the temperature gradient and the heating power calculations. The simulation also reproduced ion and electron heat

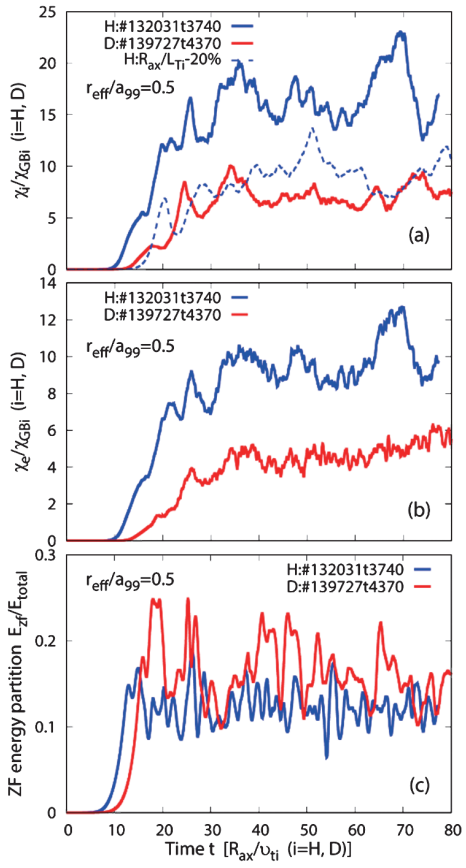

Fig. 2 Gyrokinetic simulation results of (a) normalized χ_i, (b) normalized χ_e, and (c) kinetic energy partition of zonal flow [2].

diffusivities that decreased in the D plasma. The zonal flow energy partition was higher in the D plasma, which indicates the ion mass impact on the zonal flow generation related to the transport suppression [8].

Study of energetic ion confinement by means of comprehensive neutron diagnostics

In the LHD plasma discharge with NB injection, neutrons are mainly created by beam-thermal reactions. Therefore, by using neutron diagnostics, we can obtain information of beam ions confined in the plasma. In order to understand the global confinement of beam ions, total neutron emission rate S_n is measured in plasmas with changing the magnetic axis position [4]. The line-averaged electron density n_{e_avg} dependence of S_n are surveyed in R_{ax} of 3.55 m, 3.60 m, 3.80 m, and 3.90 m (Fig. 3). The peak of S_n is seen at n_{e_avg} of 2×10^{19}-3×10^{19} m^{-3}. In outward shifted configurations, S_n is smaller by almost one order than S_n of the inward shifted configurations in the same density. One of the main reasons of lower S_n in outward shifted configuration is that the electron

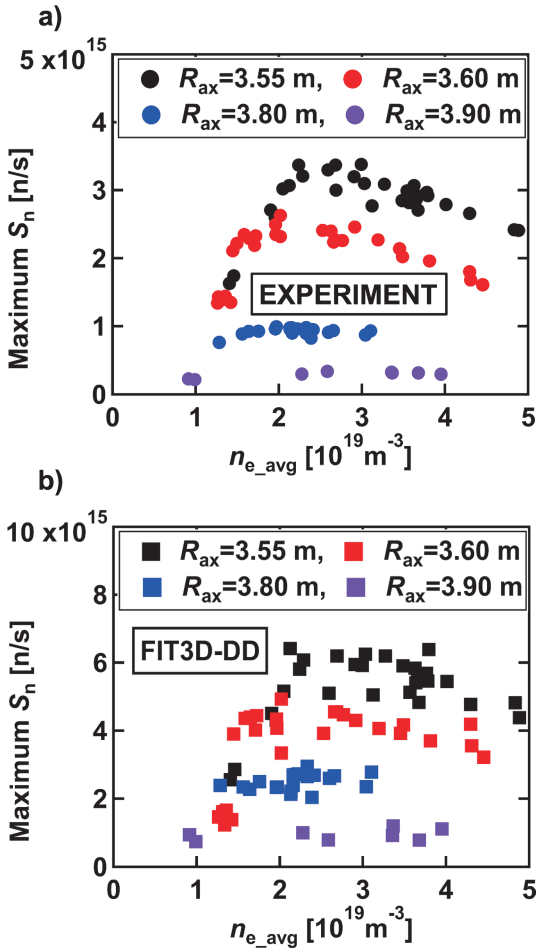

Fig. 3 The plot of the maximum S_n in one discharge as a function of n_{e_avg} in experiment (a), and FIT3D-DD code (b) [4].

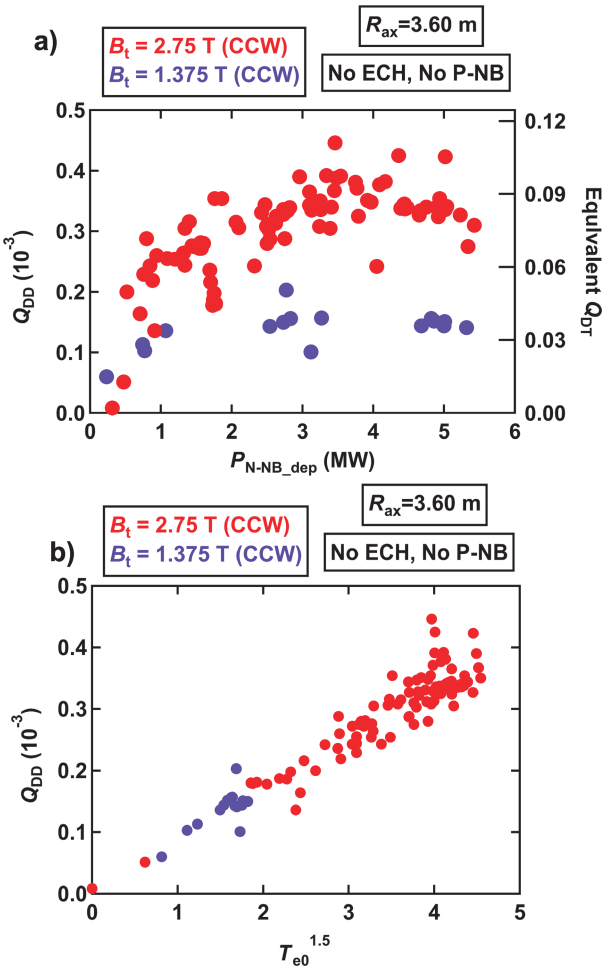

Fig. 4 (a) Q_{DD} as a function of the $P_{N\text{-}NB\_dep}$. Here, the ratio of Q_{DT}/Q_{DD} is based on FBURN calculation. (b) Relation between Q_{DD} and $T_{e0}^{1.5}$ [4].

temperature tends to be lower in the LHD plasmas with outward shift of R_{ax} which induces the shorter beam ion slowing down time. We compare experimentally obtained S_n with S_n calculated by the FIT3D-DD code which is a part of TASK3D code [9]. In FIT3D-DD code, we assumed a pure D plasma and the orbital effect of fast ion in the short time (0.1 ms) is considered. The calculated S_n dependence on n_{e_avg} shows that S_n increases with the electron density in n_{e_avg} less than 2×10^{19} m^{-3}, then has a peak at n_{e_avg} around 2×10^{19} m^{-3} to 3×10^{19} m^{-3}, and then decreases with the electron density in n_{e_avg} greater than 3×10^{19} m^{-3} as obtained in experiments. The absolute value of S_n calculated by FIT3D-DD is almost two times higher than the absolute value of S_n. The main reason of disagreement regarding absolute value may be due to the effect of the effective charge.

The NB deposition power dependence of fusion gain is surveyed in R_{ax} = 3.6 m configuration. Note that the fusion gain Q_{DD} is defined as (fusion output)/(total heating power). Here, in D plasma, the fusion output of each reaction is 7.25 MeV. We evaluate Q_{DD} in D plasma heated only by N-NB (Fig. 4). As expected, Q_{DD} in the normal B_t case is higher than Q_{DD} in the half B_t case. Gradual increase of Q_{DD} with the increase of $P_{N\text{-}NB\_dep}$ is obtained with $P_{N\text{-}NB\_dep}$ of up to 3 MW, and then Q_{DD} is almost saturated. One-dimensional neutron emission calculation code FBURN [5] is used in order to evaluate the equivalent fusion gain in DT plasma Q_{DT}. The ratio of Q_{DT}/Q_{DD} is evaluated to be 249 in triton plasma with D beam injection, which is almost the same value calculated in TFTR [10]. We achieve equivalent Q_{DT} of 0.11 which is almost the same with large tokamaks with 5 MW NB injections [10,11]. A linear increase of Q_{DD} with $T_{e0}{}^{1.5}$ is obtained in those experiments (Fig. 4 (b)). The dependence is found if neutrons are mainly created by beam-plasma reactions. When neutrons are mainly created by a beam-plasma reaction, Q_{DD} is approximately described as $Q_{DD} \sim n_i \times P_{NB} \times \tau_s / P_{NB} \sim T_{e0}{}^{1.5}$.

[1] H. Takahashi *et al*., Nucl. Fusion **58**, 106028 (2018).
[2] K. Nagaoka *et al*., Nucl. Fusion **59**, 106002 (2019).
[3] M. Nakata *et al*., Plasma Phys. Control. Fusion **58**, 074008 (2016).
[4] K. Ogawa *et al*., Nucl. Fusion **59**, 076017 (2019).
[5] K. Ogawa *et al*., Plasma Phys. Control. Fusion **60**, 095010 (2018).
[6] M. Nakata *et al*., Plasma Phys. Control. Fusion **61**, 014016 (2019).
[7] T.-H. Watanabe and H. Sugama, Nucl. Fusion **46**, 24 (2006).
[8] M. Nakata *et al*., Phys. Rev. Lett. **118**, 165002 (2017).
[9] S. Murakami *et al*., Trans. Fusion Technol. **27**, 256 (1995).
[10] D.L. Jassby *et al*., Phys. Fluids B **3**, 2308 (1991).
[11] M. Keilhacker and the JET Team, Phys. Fluids B **2**, 1291 (1990).

(K. Nagaoka, K. Ogawa and H. Takahashi)

Transport and Confinement

Highlight

Isotope effects on turbulence in ECRH plasma of LHD

The turbulence is a key player in the isotope effects of transport. Experiments were performed to compare the difference of turbulence characteristic in H and D plasma in 20th LHD experimental campaign under almost identical condition of ECRH plasma. The turbulence was measured by two dimensional phase contrast imaging [1]. Figure 1 shows the comparison [2]. The comparison of three density regimes (low (1×10^{19} m^{-3}), middle (1.8×10^{19} m^{-3}) and high (3×10^{19} m^{-3}) density regime) are shown. The line averaged density was adjusted as shown Fig. 1 (a-1), (b-1) and (c-1). The heating was 2 MW 154 GHz 2nd harmonic heating. The difference of the deposition power is less than 10%. More than 88% of injection power was absorbed at $\rho < 0.3$. Fig. 1 (a-4), (b-4) and (c-4) shows comparison of central electron and ion temperature. The central electron temperature is comparable in low and middle density regime, while it is clearly higher in high density regime. On the other hand, central ion temperature is almost the same at whole density regime. The scaling study showed that the global energy confinement time was 16% better in D plasma than in H plasma for the same line averaged density and deposition power of ECRH [1]. However, As shown in Fig. 1 (a-4), (b-4) and (c-4), the better confinement improvement is more evident at higher density regime. Figs. 1 (b) shows line integrated fluctuation amplitude from 20~200 kHz components. These are mainly come from core region at $\rho <\sim 0.8$. Figs.1 (c) shows line integrated fluctuation amplitude at 200~500 kHz components. These are mainly come from edge region at $\rho >\sim 0.8$. In low and middle density regime, core fluctuation from 20~200 kHz is higher in D plasma. However, in high density regime, core fluctuation becomes clearly lower in D plasma. The edge fluctuation from 200~500 kHz shows lower fluctuation in D plasma at all density regime, however, the difference is clearer in higher density regime. Observed lower fluctuation amplitude in D plasma possibly play a role in the better confinement in D plasma. Gyrokinetic linear analyses showed that the dominant instability was ion temperature gradient mode (ITG) at $\rho = 0.7$ [3]. The growth rate was lower in D plasma. The hollowed density gradient stabilize ITG [4]. The density profiles are hollower in D plasma [2]. The hollower density profiles in D plasma is one of the possible mechanism for the better confinement in high density regime of ECRH plasma in LHD.

[1] K, Tanaka *et al.*, Rev. Sci. Instrum. **79**, 10E702 (2008).
[2] K, Tanaka *et al.*, to be submitted Nucl. Fusion.
[3] K. Tanaka *et al.*, to be presented at EPS 2019 invited talk.
[4] M. Nakata *et al.*, Plasma Phys. Ctrl. Fusion **61**, 014016 (2019).

(K. Tanaka)

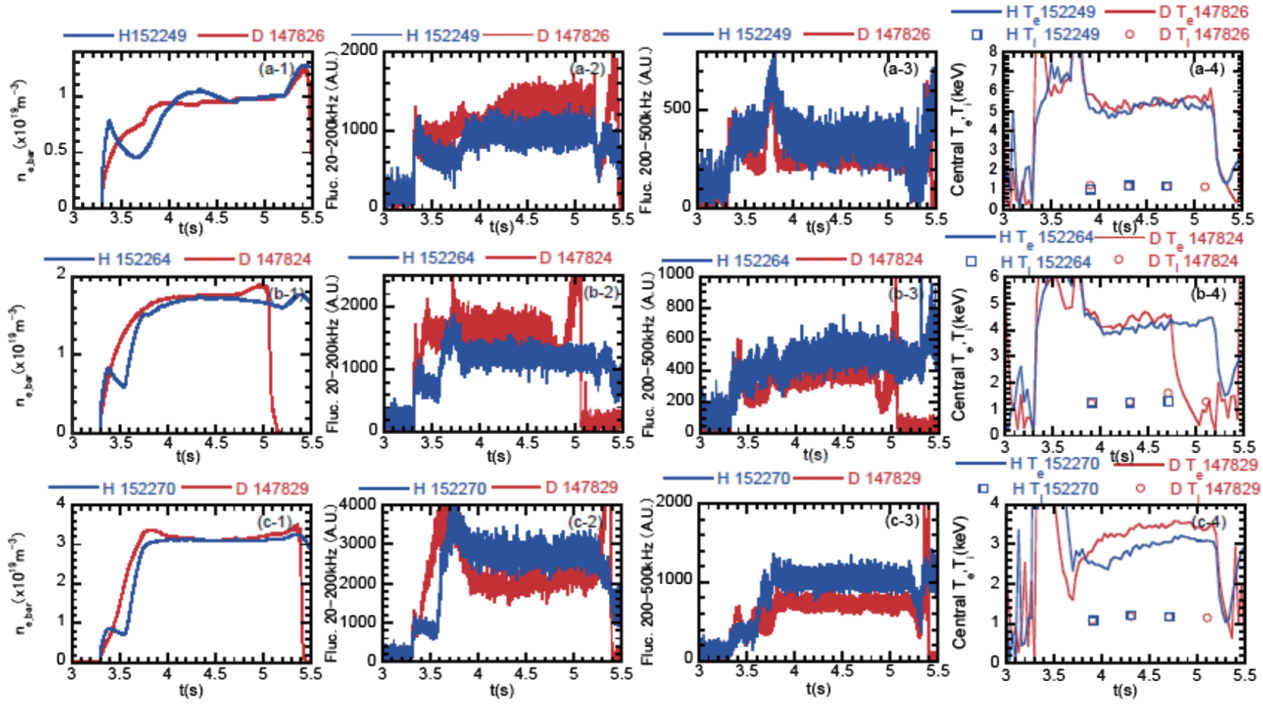

Fig. 1 Comparison of time trace in (a) low, (b) middle and (c) high density.
(a-1),(b-1),(c-1); line averaged density, (a-2),(b-2),(c-2); line integrated fluctuation amplitude for 20–200 kHz by 2D-PCI, (a-3),(b-3),(c-3); line integrated fluctuation amplitude for 200–500 kHz by 2D-PCI, (a-4),(b-4),(c-4); central electron and ion temperature at ρ = 0~0.2 measured by Thomson scattering and CXRS

Real-time injection control of ECH power in LHD

Optimum injection settings of ECH are essential for achieving desired power deposition and reducing the stray radiation level in the vessel. Since the 18th LHD experimental campaign, ray-tracing calculations with the LHDGauss code [1] have been performed on a shot-by-shot basis under the automatic analysis tool AutoAna [2] that have improved heating performance by launcher adjustment during experiments.

In the 20th campaign, we performed real-time deposition location control experiments in order to maintain high absorbed power and on-axis heating during varying electron density. The optimum target settings were calculated in advance using LHDGauss for various electron density profiles. The density profiles are characterized with densities at the magnetic axis, at the last closed flux surface, and at the shoulder for hollow profiles. Then, those parameters were calculated with multi-channel FIR laser interferometer, whose signals were inputted into the newly-developed deposition location control system with real-time FPGA (field programmable gate array) processing [3]. A demonstration was conducted for a density ramp-up case from $1 \times$ to 4×10^{19} m^{-3} as shown in Fig. 1, where the antenna control was started at 3.5 s for comparison with the case without the control. The antenna angles and the resultant target positions successfully followed their command values under the limited

motor rotation speeds. Plasmas were heated and sustained by other ECH. The absorbed power was constant during a relatively low-density case ($< 2.5 \times 10^{19}$ m^{-3}). The high absorbed power was maintained longer in the case with the control than in the case without the control from 5.5 s to 6 s at almost 3×10^{19} m^{-3}. In addition, more center-peaked deposition was maintained longer. On the other hand, no significant difference in the decreased absorbed power between the two cases was observed around 4×10^{19} m^{-3}, which suggests that the multi-pass absorption components are dominant. Pure mode excitation on the refracted wave is needed in order to increase the single-pass absorption. Extension of the high-density operational range and application to long-pulse operations will be future works.

[1] T. Ii Tsujimura *et al.*, Nucl. Fusion **55**, 123019 (2015).
[2] M. Emoto *et al.*, Fusion Eng. Des. **89**, 758 (2014).
[3] T. Ii Tsujimura *et al.*, Fusion Eng. Des. **131**, 130 (2018).

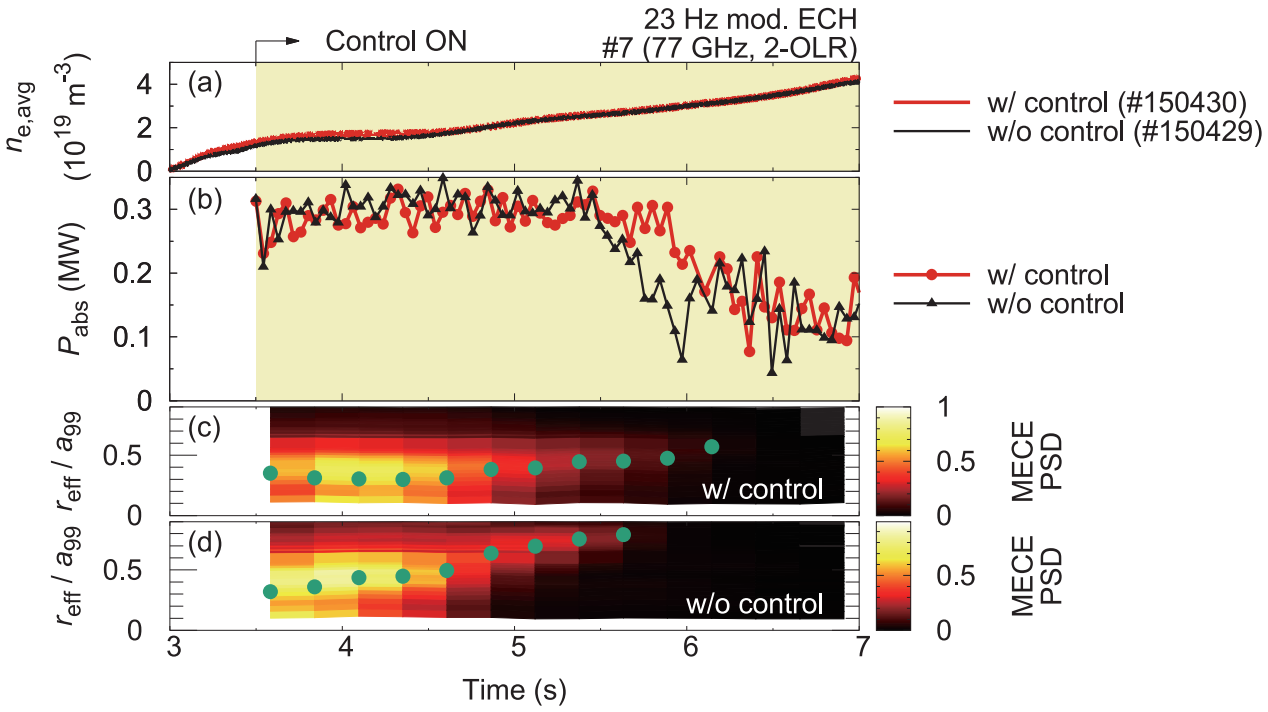

Fig. 1 Time evolution of (a) averaged electron density, (b) absorbed power, and (c)(d) radial profiles of modulation ECE signals on the cases with and without the control.

(T. Ii Tsujimura)

Edge/Device/Atomic and Molecular Processes

Highlight

Divertor tiles made of tungsten coated graphite were installed in an inboard-side divertor

Tungsten (W) is a prime candidate of the plasma facing material in a future fusion reactor. To investigate the effects of divertor tiles made of W on plasma performances, 64 divertor tiles and 30 dome tiles made of W coated graphite were installed in the 9-I closed divertor as shown in Fig. 1. A scanning electron microscopy image of a cross-section of a W coated divertor tile is shown in Fig. 2. On a graphite surface, 10 μm W layer is formed on 2 μm molybdenum (Mo) interlayer which reduce the stress caused by the difference of thermal expansion between W and graphite. Both W and Mo were deposited on graphite tiles by using magnetron-sputtering. During the 20th experimental campaign, clear effects of W released from W coated divertor tiles on the core plasma were not observed clearly by spectroscopic measurements. A filtered CCD camera which observed the 9-I divertor from 9-O port to detect released W atoms also could not observe W clearly. 9-I and other inboard-side divertors were observed by eyes in the LHD vacuum vessel after the end of the 20th campaign. As a result, much smaller amount of flakes which are exfoliated deposition layers are observed at the 9-I divertor than at the other inner divertor. This result is attributed to reduced carbon deposition on the first wall and the dome structure, which are located beside divertor tiles with W coating.

Fig. 1 W coated divertor components

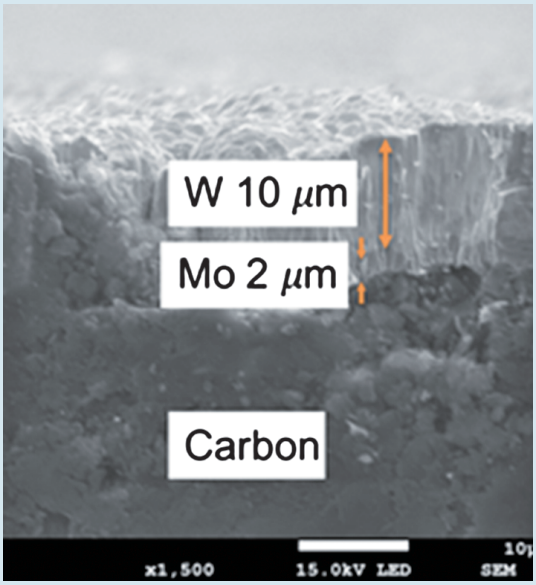

Fig. 2 A cross-section of a W coated divertor tile

(G. Motojima)

New installation of in-vessel Non Evaporable Getter (NEG) pumps for the divertor pump

Non Evaporable Getter (NEG) pumps which use the patented ZAO getter alloy [1] have been installed in the 9-I closed divertor as an in-vessel pump [2] as shown in Fig. 1. Unlike a cryo-pump, the operation temperature of a NEG pump is 100–200°C or higher. The higher operation temperature is an advantage of the NEG pump over a cryo-pump in a vacuum vessel of a fusion experimental device in which plasma facing components have to be tolerant to a plasma radiation and heat loads from heating devices. For the installation in LHD, simulations of the heat load from NEG pumps to the first wall and the conductance of neutral particles towards NEG pumps (Fig. 2) were carried out by using a finite element method based software for multi-physics analysis (ANSYS) and a fully three-dimensional neutral particle transport simulation code EIRENE, respectively. The pumping performance test was conducted in NIFS, and the result shows that the effective pumping speed for hydrogen is 10 m^3/s which is close to the required pumping speed for the in-vessel pump in LHD. In the LHD vacuum vessel, the exposure of the NEG pumps to boronization and glow discharge cleanings have been examined, and no effect of them on the pumping performance have been observed.

[1] F. Sivieroa *et al.*, Fusion Eng. Des., in press.
[2] G. Motojima *et al.*, Fusion Eng. Des. **143**, 226–232 (2019).

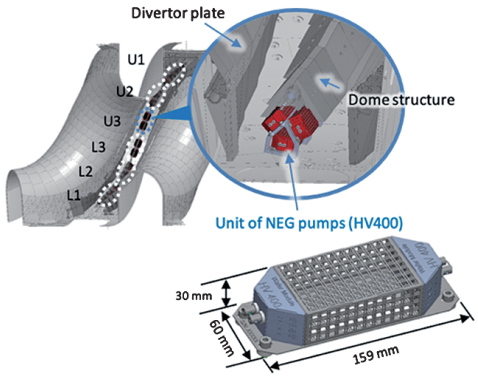

Fig. 1 A NEG pump and the arrangement of NEG pumps in the 9-I closed divertor.

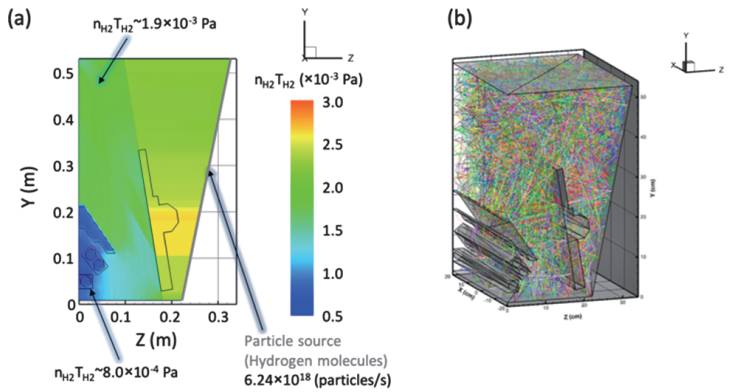

Fig. 2 A result of the simulation using the EIRENE code. (a) A pressure distribution on a cross-section of the closed divertor in which NEG pumps are installed. (b) Trajectories of test particles in the simulation.

(G. Motojima and M. Shoji)

Control of 3D edge radiation structure and compatibility with core plasma performance

The resonant magnetic perturbation (RMP) field has been applied to the LHD plasma, which creates a remnant magnetic island in the edge stochastic layer. The magnetic island is found to affect the edge plasma parameter profiles including impurity radiation. The electron temperature and pressure profiles are flattened at the island. On the other hand, the electron density is slightly peaked at the edge of the island. The impurity radiation profile is estimated assuming non-coronal cooling rate function. The time evolution of the obtained impurity radiation are plotted in Fig.1 (a), together with the magnetic field line connection length (LC) at the edge. It is found that the radiation is enhanced and fixed around the magnetic island during the detached phase, where the discharge is stably sustained with controlled level of radiation [3]. Without RMP (Fig. 1 (b)), the radiation penetrates the confinement region, leading to radiation collapse. In spite of the reduced effective plasma volume caused by the edge magnetic island and by the enhanced radiation there, the central plasma pressure finally exceeds the case without RMP. This is caused by the pressure profile peaking at the central region in the case with RMP, as shown in Fig. 2 [1]. These results indicate clear change of core plasma confinement during the detached phase with RMP.

[1] M. Kobayashi *et al.*, Nuclear Materials and Energy, **17**, 137 (2018).

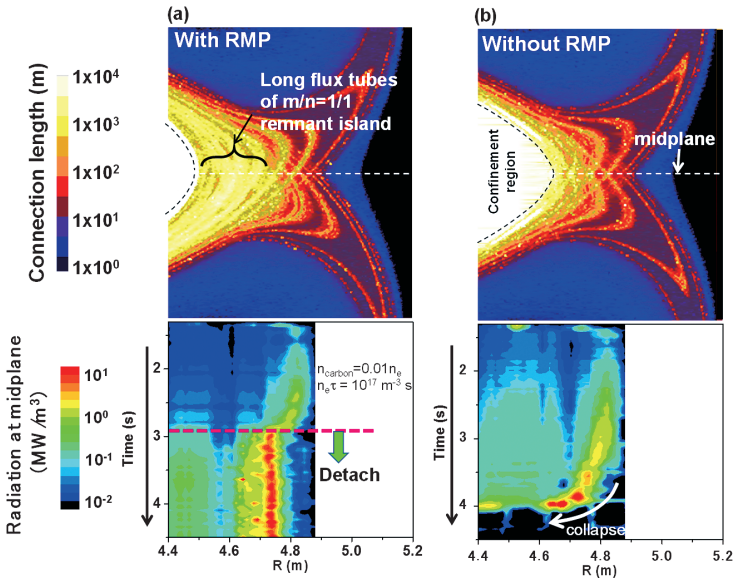

Fig. 1 Upper panels: Connection length (L_C) distributions in the stochastic layer at the outboard side. Lower panels: Temporal evolutions of carbon radiation profiles estimated from T_e and n_e of Thomson measurements, assuming spatially constant carbon concentration of 1% and non-coronal cooling rate ($n_e\tau = 10^{17}$ m^{-3} s). (a) With RMP (#85946), (b) without RMP (#85948). [1]

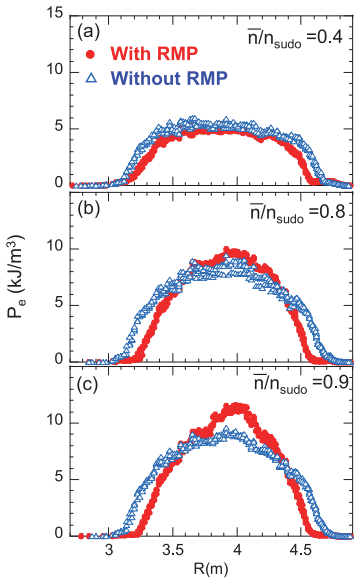

Fig. 2 Radial profiles of electron pressure at $\bar{n}_e/n_{sudo}$ = 0.4, attached, (a), 0.8, detached, (b), and 0.9, detached, (c), respectively. Red: with RMP, blue: without RMP application. [1]

(M. Kobayashi)

High-β/MHD/Energetic Particles

Highlight

Impact of ECH/ECCD on fast-particle-driven MHD instabilities

Fast particle (FP)-driven magnetohydrodynamics (MHD) instabilities enhance anomalous transport and/or induce the loss of fast particle including alpha particles in a fusion reactor. Since redistribution and exhaust of alpha particles lead to reduction of fusion gain Q and damage of first wall, it is required to establish methods of stabilization and/or control of FP-driven MHD instabilities for the fusion reactor, but they have not been established yet. Electron cyclotron heating (ECH)/electron cyclotron current drive (ECCD) are a candidate method to control the FP-driven MHD instabilities because ECH/ECCD may be an ideal tool to control the modes since they can provide highly localized EC waves with a known location and good controllability [1-3]. A linear MHD theory predicts that the changes in electron density and temperature by ECH and in plasma current by ECCD can affect both the growth and damping rates of the FP-driven MHD instabilities.

We have applied ECCD to an NBI plasma on LHD in order to mitigate and eventually suppress the observed FP-driven MHD instabilities. Figure 1 shows clear destabilization and stabilization of GAEs and TAEs with frequency f_{obs} > 100 kHz, and EPMs with f_{obs} < 100 kHz in the LHD plasma with high magnetic shear s when magnetic shear at plasma core is decreased and increased by co- and counter-EC driven plasma current, respectively. The main differences in plasma parameters between both cases are plasma current and magnetic fluctuations. The difference in the amplitude of plasma current can lead to the difference of shear Alfvén continua in whole plasma region. According to reconstructed MHD equilibrium, which qualitatively agrees with the measurement of rotational transform profile by motional stark effect (MSE) diagnostics, co-ECCD and counter-ECCD induced the co and counter plasma current whose profile peaked at plasma core. This increases and decreases the rotational transform, and then magnetic shear will be decreased and increased by co- and counter-ECCD. For co-ECCD, the TAE gap in shear Alfvén continua is aligned from the core toward the edge and many discreate eigenmodes corresponding to TAE and GAE can exist. On the other hand, for counter-ECCD, discrete eigenmodes tend to cross the shear Alfvén continua leading to continuum damping.

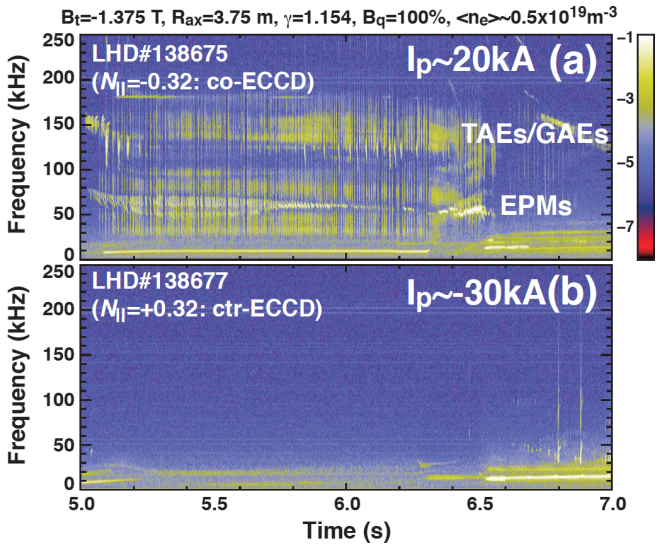

Fig. 1 (a) Destabilization and (b) stabilization of TAEs, GAEs and EPMs due to co- and counter-ECCD in the NBI-heated LHD plasmas. Plasma current is ~20 kA which decreases s in (a) and ~–30 kA which increases s in (b).

[1] K. Nagaoka *et al.*, Nucl. Fusion **53**, 072004 (2013).
[2] K. Nagasaki *et al.*, Nucl. Fusion **53**, 113041 (2013).
[3] S. Yamamoto *et al.*, Nucl. Fusion **57**, 126065 (2017).

(K. Nagaoka)

Suppression of the EIC modes with the m/n = 1/1 RMP

The confinement of energetic particles is essential for the realization of the magnetically confined fusion reactor. Energetic particles are not well confined when the EP driven MHD modes are excited, such as the helically-trapped energetic-particle (EP) driven resistive interchange mode (EIC) [1] observed in LHD. Strategy and the initial results to suppress the EIC mode are presented.

The rotational transform of the LHD device is created by the two helical coils (L=2/M=10). As a consequence, helically twisting region where the magnetic field strength is weak appears. EPs having perpendicular velocity components are trapped in this region and make precession motion helically. The rotation frequency of this precession motion is slow enough to interact with the pressure driven MHD modes.

Two methods to control the EIC have been tested on LHD. One is the ECH application [2]. With the increase of the electron temperature at the mode rational surface, the mode width of the resistive MHD mode becomes narrower. The interaction of the trapped EPs and the MHD mode becomes thereby smaller. This method is quite effective and one of the highest-Ti with high-Te discharge is produced by this method.

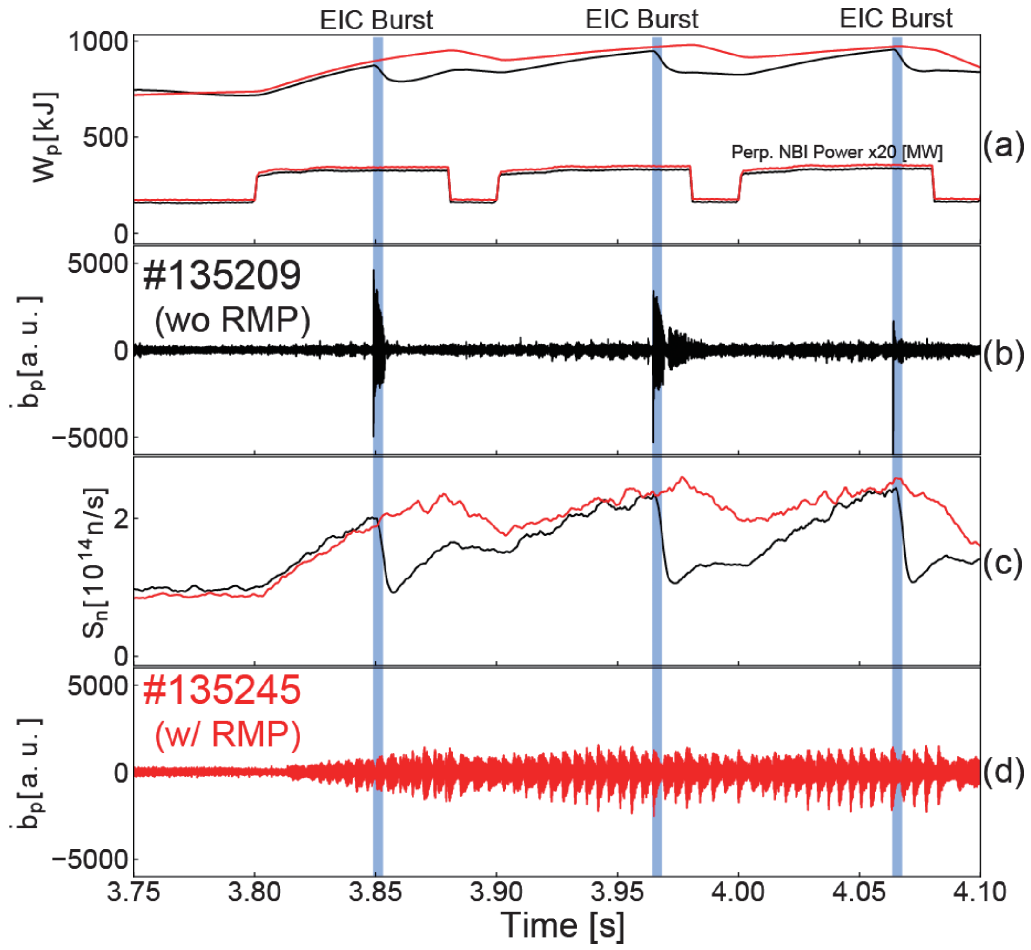

Fig. 2 Comparison of the plasma parameters with (#125245 red lines) and without (#135209 black lines) the RMP field. Heating patterns and the plasma stored energy are shown in (a). The magnetic fluctuations are shown in (b) and (d), and the total neutron emission rate is shown in (c).

Another controlling scheme, resonant magnetic perturbation (RMP) applications is also performed [3]. Bursts of the magnetic fluctuations, which cause the loss of EPs, disappear when the RMP field (m/n = 1/1) is applied as shown in Fig. 2. Small-scaled chirping-up coherent modes remain. However, these magnetic fluctuations do not trigger the bursting EIC modes which cause the EP loss, as shown in the Fig. 2 (c). From the systematic survey of the RMP application in the hydrogen beam experiments, it was found that the EIC bursts completely disappear when the RMP field is sufficiently large. Detailed mechanism of the suppression has not been clarified. However, since the MHD activities having the resonant frequency is reduced with RMP, it is likely EICs are suppressed from the stabilization of the bulk resistive interchange mode by the formation of the magnetic island caused by the RMP.

[1] X. D. Du, *et al.*, Phys. Rev. Lett. **114**, 155003 (2015), Nucl. Fusion **56**, 016002 (2016).
[2] X. D. Du, *et al.*, Phys. Rev. Lett. **118**, 125001 (2017).
[3] S. Ohdachi, *et. al.*, "Excitation mechanism of the energetic particle driven resistive interchange mode and strategy to control the mode in Large Helical Device", in proc. 27th IAEA Fusion Energy Conference, Gandhinagar, India, Oct. 22–27 2019, https://nucleus.iaea.org/sites/fusionportal/Shared%20Documents/FEC%202018/fec2018-preprints/preprint0128.pdf.

(S. Ohdachi)

Study of slowing down mechanism of locked-mode-like instability in helical plasmas

The locked-mode-like instability is one of the MHD instabilities observed in the LHD and it leads to minor collapse after a precursor slows down. In the LHD, there are two types of the locked-mode-like instability categorized by the difference of the radial structure of the precursor. The instability with the odd function type structure is called 'type-I instability' and the instability with even function type structure is called 'type-II instability'. The type-I/II instability is considered to have a large/small magnetic island. The slowing down mechanism of both instabilities, which may be related to the occurrence of minor collapse, has been investigated through the experimental analysis.

Figure 3 (a)–(e) show typical waveforms of a discharge with the type-II instability. In this discharge, the intrinsic error field is almost suppressed. After the precursor with the m/n = 1/1 structure appears at t ~ 3.8 s, the mode frequency f_{mode} and the mode amplitude are almost constant until 4.2 s (constant phase). Then, the f_{mode} gradually decreases and the mode amplitude increases (slowing down phase). Finally, the f_{mode} becomes almost zero at 4.56 s. Comparing the f_{mode} with the $\boldsymbol{E} \times \boldsymbol{B}$ rotation frequency at the resonant surface $f_{\boldsymbol{E} \times \boldsymbol{B}}$, the f_{mode} and the $f_{\boldsymbol{E} \times \boldsymbol{B}}$ are almost the same from the constant phase to the slowing down phase. It suggests that the precursor rotates with the $\boldsymbol{E} \times \boldsymbol{B}$ plasma flow. By investigating the relationship between the $f_{\boldsymbol{E} \times \boldsymbol{B}}$ profile and the resonant surface location, it is found that the slowing down phase consists of the following two stages. Figure 3 (e) shows the time evolution of the radial profile of the $\boldsymbol{E} \times \boldsymbol{B}$ rotation frequency (filled areas) and the resonant surface location (closed circles). Figure 3 (f) shows the radial profile of the $\boldsymbol{E} \times \boldsymbol{B}$ rotation frequency at three timings. In the first stage, such as t = 4.28 and 4.38 s, the resonant surface moves toward the plasma core region (R = 4.16 m

to $R = 4.06$ m), where the $\boldsymbol{E} \times \boldsymbol{B}$ rotation frequency is small. In the second stage (just before $t = 4.58$ s), the $\boldsymbol{E} \times \boldsymbol{B}$ rotation frequency near the resonant surface becomes small. Such a slowing down process is similar to that of the type-I instability [1]. This result suggests that the effect of the magnetic island size on the slowing down of the locked-mode-like instability in the LHD is not significant.

[1] Takemura Y. *et al.*, 2017 Plasma Fusion Res. **12**, 1402028–1402028.

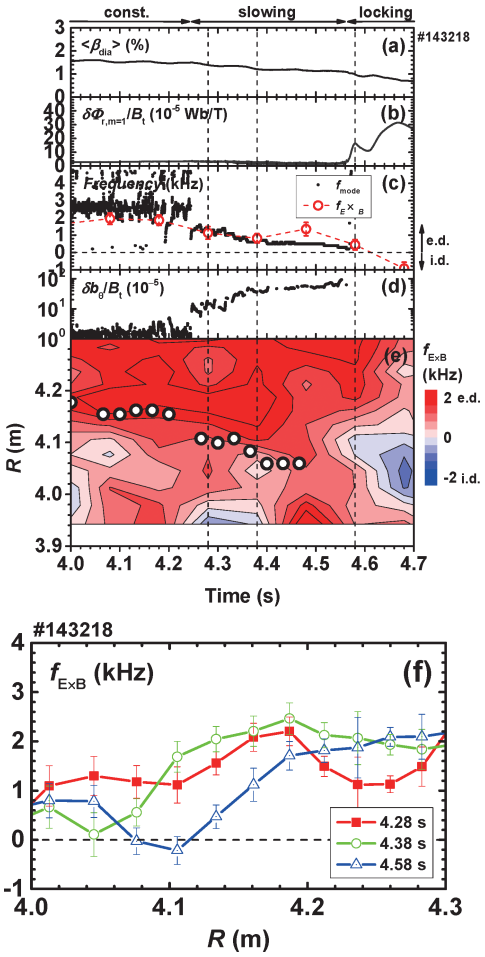

Fig. 3 Time evolution of (a) volume-averaged beta value, (b) radial mode amplitude by saddle loop coils, (c) mode frequency f_{mode} by a magnetic probe (closed circles) and $\boldsymbol{E} \times \boldsymbol{B}$ rotation frequency $f_{E \times B}$ at $\iota/2\pi = 1$ resonant surface (open circles), (d) poloidal mode amplitude by a magnetic probe and (e) radial profile of $\boldsymbol{E} \times \boldsymbol{B}$ rotation frequency and location of $\iota/2\pi = 1$ resonant surface (closed circles). (f) radial profile of $\boldsymbol{E} \times \boldsymbol{B}$ rotation frequency at each time corresponding to vertical lines in Fig. 1 (a)–(e) in the almost-reduced error field discharge. A positive (negative) sign of Fig. 1 (c) and (f) means an electron (ion) diamagnetic direction. The red (blue) area in Fig. 1 (e) corresponds to the electron (ion) diamagnetic direction.

(Y. Takemura and Y. Suzuki)

Research and Development Collaboration Program for LHD-Project

A special collaboration program, which is aimed to support the research and development activities in domestic universities for advanced diagnostics or heating scenarios, is established for future application on the LHD. Two examples of such activities are shown in this section.

a) Hydrogen recycling Model on carbon divertor by molecular dynamics simulation for neutral transport analysis in LHD

When the divertor plates are irradiated by hydrogen ions, some hydrogen atoms and molecules reflect back to the plasma while the other hydrogen atoms are retainedretain in the divertor. These recycled neutral hydrogen atoms and molecules affect the plasma parameter of the core plasma by ionization and charge-exchange reaction caused during their travel to the core plasma via edge plasma. Moreover, in the situation of rising expectations of the detached divertor, recent research revealed that the recombination processes caused by hydrogen molecule, the so called molecular assisted recombination (MAR), plays an important role for the neutral transport in the edge plasma. In particular, the effects of charge exchange recombination and dissociative recombination cannot be ignored for an understanding of the process of the neutral transport at the edge plasma.

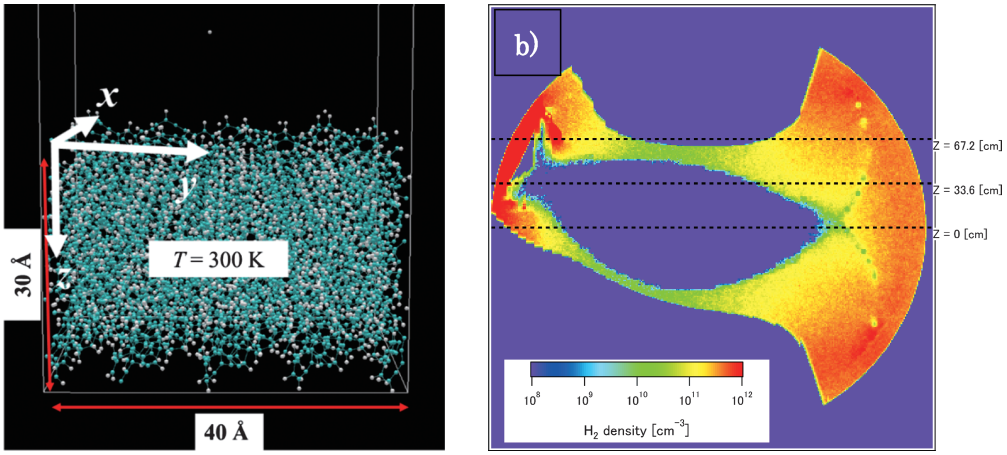

Fig. 1 (a) Molecular dynamics simulation model of carbon and hydrogen atoms. (b) Special distribution of hydrogen molecules density in LHD calculated by new neutral-transport code with developed hydrogen recycling model on carbon divertor.

The transport of the neutral particles can be numerically simulated by neutral-transport code. However, conventional neutral transport codes cannot treat the process of MAR. To avoid this problem, the Shinshu University group is now developing a new neutral-transport code which can treat the process of MAR. In order to provide the information of recycled hydrogen atoms and molecules the neutral-transport code, we have developed [1, 2] a simulation model for hydrogen recycling process on carbon divertor. Our recycling model consists of two regions: MD and HC regions. The inside (MD region) and the outside (HC region) are governed by equations of motion, that is, molecular dynamics (MD) simulation, and heat conduction equation, respectively. In the MD region, as shown in Fig. 1(a), one hydrogen atom is injected into a hydrogen containing amorphous carbon material. Because of the computation time, it is impossible to prepare the MD region large enough to calculate

the process of heat transfer to the bulk which is caused by the kinetic energy entering the target material with the injected hydrogen atom.

The information of emitted hydrogen atoms and molecules are investigated. By multiple trials, the distributions of emission angle, translational energy, vibrational states, and rotational states of emitted hydrogen atoms and molecules are obtained. Code integration of neutral-transport code and our developed hydrogen recycling model is successfully performed as shown in Fig. 1(b).

(S. Saito, Yamagata University)

b) Development for advanced turbulence diagnostics and analyses for magnetically confinement plasmas

The understanding of plasma confinement has made great progress. However, there still are many unsolved problems, such as isotope effects, non-local transport, origins of improved confinement, and background physics for empirical scaling laws. The studies of plasma turbulence are the keys for solving these issues, and the new concepts to understand the plasma turbulence, 'cross-scale couplings' and 'symmetry-breaking' in plasma turbulence, have been proposed to require new and advanced diagnostics for plasma turbulence in order to measure the entire cross-section, at least two dimensions, of plasma. The present collaboration work is undertaking research and development of a tomography system as such a diagnostic in terms of hard- and software.

The turbulence tomography was newly installed on PANTA, a linear cylindrical plasma device in Kyushu University. The diagnostic enables obtaining two-dimensional image of plasmas using 6 directional linear visible imaging systems. Several new analyzing methods were newly developed to quantify the images, such as Fourier-Bessel analysis with optimized choice of the fitting bases [3], and fast algorithm for monitoring images using Tikhonov regularization [3]. The application of the Stokes parameters, known as the indexes to quantify polarization characteristics in optics, has been recently proposed for quantifying the rotation characteristics of azimuthal modes [4]. The method successfully extracts the rotation properties of fluctuation patterns that appear in the turbulent plasmas. It is found, as is shown in Fig. 2, that broad-band fluctuations could show clear polarization characteristics as well as coherent fluctuation patterns in a region of plasma. Further, a Tikhonov method using L1-regularization [5], Time Delay Estimate (TDE) Fourier-Rectangular analysis [6], and others are being developed.

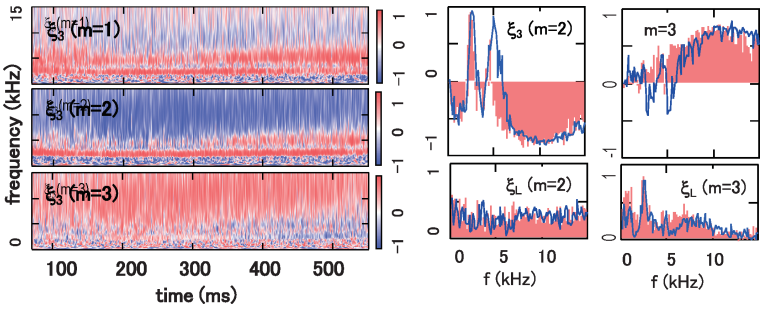

Fig. 2 Examples of Stokes parameter analysis of azimuthal mode dynamics. Here the azimuthal modes of m=1, 2, and 3 are analyzed. Stokes parameters are calculated using the moments of emission distribution.

(A. Fujisawa, Kyushu University)

[1] H. Nakamura *et al.*, 18th ICPP, Taiwan (2016).
[2] S. Saito *et al.*, Proceedings of 37th JSST (2018).
[3] K. Yamasaki *et al.*, Rev. Sci. Instrum. **88**, 93507 (2017).
[4] A. Fujisawa *et al.*, Phys. Plasmas **26**, 012305 (2019).
[5] K. Yamasaki *et al.*, Rev. Sci. Instrum. **88**, 93507 (2017).
[6] K. Yamasaki *et al.*, J. Appl. Phys., being submitted.